DECLINE OF GIANT IMPACTS ON MARS BY 4.48 BILLION YEARS AGO AND AN EARLY OPPORTUNITY FOR HABITABILITY

Authors: D.E. Moser[1*], G.A. Arcuri[1], D.A. Reinhard[2], L.F. White[3], J.R. Darling[4], I.R. Barker[1], D.J. Larson[2], A.J. Irving[5], F.M. McCubbin[6], K.T. Tait[3], J. Roszjar[7], A. Wittmann[8], C. Davis[1]

Affiliations:
[1] Department of Earth Sciences, University of Western Ontario, London, Ontario N6A 5B7, Canada
[2] CAMECA, Madison, WI 53711, USA
[3] Department of Natural History, Royal Ontario Museum, 100 Queens Park, Toronto, Ontario M5S 2C6, Canada
[4] School of Earth and Environmental Sciences, University of Portsmouth, Portsmouth PO1 3QL, UK
[5] Department of Earth and Space Sciences, University of Washington, Seattle, WA 98195 USA
[6] NASA Johnson Space Center, Mailcode XI2, 2101 NASA Parkway, Houston, TX 77058, USA
[7] Department of Mineralogy and Petrography, Natural History Museum Vienna, Vienna, Austria
[8] Eyring Materials Center, Arizona State University, Tempe, AZ 85287-1704, USA

*Correspondence to: desmond.moser@uwo.ca

A first step to understanding the initial conditions for habitability pathways in planetary systems is to determine when heavy meteorite bombardments waned and the earliest crust remained below the known thermal and shock pressure limits on microbiota survival (121°C, 78 GPa). We have determined this timing on Mars by documenting the metamorphic histories of its oldest known, 4.476 Ga to 4.430 Ga, grains of the highly resilient minerals zircon and baddeleyite in the Rabt Sbayta polymict breccia meteorites; crustal fragments of the southern highlands. Here we show using electron and atom probe microscopy that the Mars grains (n=121) have all remained beneath 78 GPa conditions, with 97% exhibiting weak to no shock metamorphic features, or thermal overprints due to shock-induced melting and magmatism. This is opposite to bombarded crust on Earth and Moon wherein ~80% of grains show such features. The nearly pristine state of the Mars minerals thus establishes a lower age bracket of 4.48 Ga for the planet-scale impact that created the hemispheric dichotomy, and obviates any later cataclysmic bombardments. Considering existing thermal habitability models, portions of early Mars crust reached habitable conditions by at least 4.2 Ga, the onset of the martian 'wet' period, as much as ~500 million years earlier than the earliest record of life on Earth. An early giant impact period on Mars, broadly coeval with Moon formation, may have heralded early abiogenesis on both planets.

The search for evidence of life on Mars continues to be a focus of planetary research, and recent work[1] has heightened interest in the age range of crust that could have hosted life. Determining the earliest time window of martian habitability, however, requires measurement of the age at which the earliest crust transitioned permanently to a state in which both the intense shock pressures and heat (direct and indirect) caused by the early impact bombardment epoch subsided below viability thresholds for Earth-like deep biosphere[2,3]. Ultimately this transition depends on the timing and rate of delivery of impact energy to the inner solar system, a poorly constrained quantity ranging from exponential decline from the time of planet accretion at 4.56 Ga and Moon formation at ~4.50 Ga[4,5] to a later pulse at 4.0 Ga to 3.8 Ga due to proposed gas giant migration; the hotly debated late heavy bombardment (LHB)[6]. Thermal habitability windows for hypothermophiles range correspondingly; from transient episodes between 4.4 Ga and 4.1 Ga, to a much later window at 3.8 Ga[3]. Shock pressure waves of tens of GPa created by bombardment can also frustrate life, however experiments reveal thresholds for survival as high as 78 GPa[7] with resilience for pressure-adapted bacteria[8]. Here we present a test of which bombardment scenario applies to early Mars by reconstructing the maximum shock pressures and temperatures experienced on Mars by zircon and baddeleyite from the oldest known martian crust within the Rabt Sbayta Martian polymict breccia meteorites in combination with recent thermochronology[9].

Zirconium minerals as metamorphic indicators

Zircon and baddeleyite are relatively common accessory minerals in planetary crusts and are known to faithfully record large length-scale (hundreds of kilometers) and large magnitude thermal and pressure perturbations that are otherwise erased in the rock record[10]. Micro-scale effects of heat (>400°C) include resorption of crystal facets, micro-zircon growth, and/or epitaxial overgrowths of metamorphic zircon[11] or, in the case of baddeleyite, rounding and truncation of igneous zoning and/or replacement by zircon[12]. At the nano-scale, atom probe tomography (APT) shows that high temperature (>800°C) metamorphism causes clustering of trace elements such as Pb, Al and Y[13,14]. Extreme heat (>900°C) resulting from shock waves >40 GPa[15] also produce diagnostic micro-features. In zircon these include curviplanar fractures, partly lined with impact melt, partial to total conversion to granular neoblasts[10,16], or, in impact melt sheets and ejecta blankets, breakdown of zircon to ZrO_2 and silica[17].

The micro- and nano-scale indicators of shock pressure ≥40 GPa differ for zircon and baddeleyite. Zircon micro-scale features include lamellae or granules of the high-pressure polymorph reidite[18]. Baddeleyite is more sensitive to shock pressure than most rock-forming minerals, exhibiting microscopic, orthogonally-related reversion twins following shock above 5 GPa[19], and grains at pressures above >29 GPa are converted to defect-rich, nanocrystalline assemblages as seen in young martian meteorites[20]. At the nano-scale, shock metamorphism of baddeleyite combined with indirect heating to ~750°C by a kilometres-thick melt sheet caused nanoclustering of trace elements U, Fe, and Mn[21], whereas zircon at >40 GPa and 900°C exhibits nanoclustering of Pb and Al (see below). These features can survive post-impact annealing effects that otherwise erase shock effects in rock-forming minerals (quartz, plagioclase)[10] as well as fluvial and glacial surface transport following crater erosion[22]. We have compared this large suite of indicators of pressure ≥5 GPa and temperatures >400°C to the properties of individual zircon and baddeleyite grains from early Mars preserved in the meteorite North West Africa (NWA) 7034[23] and paired meteorites (collectively, the "Martian polymict breccia" meteorites).

Meteoritic crustal fragments of early Mars

The Martian polymict breccia meteorites are recognized as a rare sample of the martian regolith[24], launched most likely from Mars' southern highlands[24–26], that consists of clasts of impact melt together with crystal and lithic fragments of Mars' oldest crust[24,27,28]. The chronology and lithologic makeup of these paired stones have been studied by numerous groups, and some common elements in their evolution have become apparent. The breccia contains diverse clasts of crystalline igneous, sedimentary, and vitrophyric rocks[24,26,29] that were assembled and welded[29] during a high energy event that produced melt clasts and impact spherules with impactor component[24]. The age of this impact event was initially estimated at ~1.4 Ga[25,29], although recent thermochronology suggests a date as young as 0.2 Ga[9]. Launch to Earth occurred at least 5 million years ago[9,30]. The launch event exposed the meteoroid to shock pressures between 5 and 15 GPa, creating open fractures that presently cross-cut all components of the meteorites. These were infilled by carbonate during residence in the Rabt Sbayta region of the Saharan desert where the meteorites were recovered[25,29,31].

The oldest lithic clasts are fine-grained noritic to monzonitic igneous rocks and a subset of fine-grained sedimentary rocks[25,29]. These clasts are the hosts of accessory zircon and baddeleyite, and we focus on these as they are the oldest known martian minerals and are capable of preserving the highest fidelity record of shock metamorphism. Two populations of crystalline zircon were recognized with ages of 4.476 ± 0.001 Ga and 4.430 ± 0.001 Ga, respectively[28]. Baddeleyite yielded U-Pb ages in the range of the younger population of zircon[24,29]. Raman spectroscopy ($\nu_3(SiO_4)$) and photoluminescence (Dy^{3+}) of crystalline zircon (n = 10) from NWA 7906 and NWA 7475 reveal zoning in crystallinity due to varying radiation damage (U concentration), but no evidence of zircon transformation to the high-pressure polymorph reidite[32]. Here we present a systematic assessment of the thermal and shock history of a larger population of zircon and baddeleyite grains to compare with those from bombarded Earth and Moon crust.

Shock metamorphic reconstructions

A total of nine polished surfaces from five paired stones (NWA 7034, 7475, 7906, 11220, and Rabt Sbayta 003 (Figs. S1,2,3) were scanned with an automated SEM-BSE-EDS method (see Methods). The population comprises 95 zircon and 52 baddeleyite grains (Table S1), with 40% of zircon and 53% of baddeleyite occurring within igneous clasts. Radiation damage in a U-rich subset of the zircon population [n = 26; mostly crystal clasts except where in sedimentary clasts of NWA 7034[29]] obscured internal zoning, and these grains were not considered in our study beyond inspecting grain outlines for signs of metamorphic forms (e.g., rounding, granular neoblasts). All zircon grains in lithic clasts were found to have either typical prismatic form (Fig. 1) or irregular forms ranging from euhedral to conformable with boundaries with host grains (Fig. S4). Zircon crystal clasts are generally anhedral, with some retaining one to two faceted surfaces. Metamorphic features were noted in the rounded form of two crystal clasts (although surface transport is another possibility for one grain) and a fractured igneous clast with ~300 nm wide possible metamorphic overgrowths (Table S1). The internal microstructures of the zircon and baddeleyite populations are dominated by primary zoning consistent with an igneous origin. Internal zoning in crystal clasts is frequently planar, and truncated at margins indicating that they were parts of larger igneous grains. Many crystal clasts were likely released into the fine grained matrix through comminution of igneous clasts during high energy deposition of the breccia (Figs. S4,5). The observations are similar for baddeleyite as grains within rock clasts exhibit euhedral to subhedral habit, and concentric internal zoning (Fig. S7). Crystal clasts of baddeleyite are more subhedral to anhedral but exhibit the same internal zoning as within lithic clasts (Fig. S9) and lithologies representing a younger martian crust[33].

High resolution electron backscatter diffraction (EBSD) mapping of 69 zircon grains, including 4.3 Ga grains[29], revealed two categories of lattice orientation change. Almost all grain deformations are discrete (1° to 10°) offsets across recent, open fracture sets, often conjugate, that are continuous with the launch-related fractures of host minerals and matrix (Fig. 1, Figs. S4,5). Zircon between the fractures often exhibits low, 1° to 3°, crystal plastic deformation (Fig. S6) that could be related to launch or a pre-launch shock event that created the co-existing spherules in the breccia. One zircon grain was found to exhibit clear pre-launch shock deformation, manifest as a set of planar deformation bands (Fig. S11) representing a minimum shock loading in the range of 10 GPa to 20 GPa based on Earth analogues[10]. These shock-induced microstructures formed on Mars as they are clearly cross-cut by, and therefore pre-date, launch-induced fracturing In summary, 98% of zircon grains exhibit a state of no to low (<10 GPa) shock pressure metamorphism incurred during their time on Mars.

All 29 baddeleyite grains analyzed by EBSD exhibit some combination of primary and shock-related twin domains. The primary igneous twinning is the same as that observed in terrestrial baddeleyite [i.e. {100} and {110} twins[34]] (Table S1). It is overprinted by µm to sub-µm subgrains separated by either straight, high angle twin boundaries (18°/{001}) or irregular, curved boundaries. In some grains, these discontinuous boundaries host domains with weak diffraction. The majority of grains (n = 26) displays three orthogonally related (90°) groupings of orientations in {100}, {010} and {001}, as seen in the pole figures of Figs. S8, S10). In four grains (NWA 7475; F6396, F14987, F3590, F3244; Table 1) these relationships are defined by a small number of data (50-120 nm) in the EBSD map. For all orthogonally twinned grains, a single group of orientations forms 18° cross shapes. The remaining two orientation groupings are either tightly clustered (<3°) or linearly spread / loosely clustered (<10°), due to low magnitude (1-5°) crystal plastic deformation (e.g. NWA 7475, F28444 {001}). These crystallographic features are comparable to those observed in baddeleyite exposed to shock metamorphism in the 5 to 20 GPa regime, as calibrated at the Sudbury impact structure (Canada)[19]. Two metamorphosed baddeleyite crystal clasts were identified exhibiting replacement rims of zircon (Figs. S12,13), likely due to heating and reaction with silica-rich melt prior to emplacement in breccia (Fig. S12).

Atom probe tomography (APT) was carried out on two zircon grains and two baddeleyite grains from Mars to test for nano-scale clustering of Pb and Al as seen in high temperature (>900°C) shock metamorphosed terrestrial zircon (Fig. S14). Three microtips of a euhedral zircon grain in a lithic clast (Fig. S5,) and one microtip from a subhedral igneous zircon crystal clast (Fig. S6) have mass spectra that match those of terrestrial reference zircon[35] and exhibit uniform distributions of the trace elements Al and Y (Figs. S5,6). Likewise, APT analysis of euhedral baddeleyite attached to ilmenite (Fig. S7) and a baddeleyite crystal clast (Fig. S9) yielded mass spectra that match reference terrestrial baddeleyite[35] and exhibit homogeneous trace elemental distributions of Fe and U. These nano-scale data agree with micro-scale zircon and baddeleyite observations and the metamorphic state of the host minerals; all indicate predominantly low-grade (<10 GPa, <450°C) shock and thermal metamorphic conditions throughout the >4.43 billion history of the crustal terrain that sourced the igneous clasts in the breccia.

Comparison of the microstructure and Pb-loss characteristics of these grains to those from impacted crusts on the Earth and Moon show a marked difference (Table 1). Zircons from across the meta-igneous crust of the ~100 km diameter central uplift of the largest known impact on Earth, the Vredefort dome[36], exhibit micro-features of >20 GPa shock metamorphism in 87% of grains (Table 1). Lunar zircon surveys reveal that the majority (71%) of >4 Ga grains in Apollo impact breccias[16,37] show such features. The opposite case is found for the martian polymict breccia wherein 98% of the zircons show weak to no shock deformation >20 GPa during Mars residence. Likewise the baddeleyite grains exhibit microstructures that match those in weak to moderately shocked domains of young martian shergottite, but none of the features of grains near their launch-generated melt pockets[20]. This remarkably low-intensity shock history for early Mars accessory minerals is in concert with the reported U-Pb systematics which fail to reveal impact-related Pb-loss[10] and instead preserve ancient, concordant (U-Pb) ages of 4.428 ± 0.025 Ga[24], and up to 4.476 ± 0.001 Ga[28] for zircon, and as old as 4.382 ± 0.06 Ga for baddeleyite[29] (Table S4).

Early giant impact and opportunity for abiogenesis

By pairing recent chronological constraints[9,28] with our nano-and microstructural measurements we can refine the history of Early Mars with regard to the timing of maximum impact flux on its earliest stable crust and the time at which that crust reached habitable conditions. Recent high-precision geochronology of NWA 7034 zircon grains reveals a precursor 4.55 Ga andesitic crust on Mars that melted to crystallize a secondary crust over a 50 million year span of igneous activity between 4.476 ± 0.001 Ga and 4.430 ± 0.001 Ga[28]. It is likely that the baddeleyite has a similar paragenesis, as it has an age range that is similar to zircon, is known to crystallize from mafic magmas that solidify earlier in crustal differentiation sequence, and is the dominant zirconium phase in igneous rocks from Mars[38]. The low shock levels of most of the accessory minerals are consistent with the co-existence of primary, crystalline plagioclase in igneous clasts hosting zircon (e.g., Fig. 1) and the low shock state of rock-forming minerals in general[26]. Exsolution lamellae in pyroxene and ilmenite in crystal and lithic clasts of the host rocks may indicate residence of the parent terrain near the surface of Mars[25,26], and thermochronology data indicate an upper crustal residence since 4.3 Ga[9]. Taken together, the zircon and baddeleyite population in Martian polymict breccia meteorites and their host rocks derive from a crustal terrain that did not experience moderate to high shock pressures (20 - 80 GPa), regional or local thermal (>450 °C) effects, or Pb-loss after 4.476 ± 0.001 Ga, the age of the oldest concordant zircon. These observations provide useful brackets on the timing of giant impact and habitability on early Mars.

Calculations of heat thresholds for early life during bombardment relate to the energy-release of impactors, and an impactor diameter of 500 km is sufficient to eliminate survivable conditions for deep thermophiles on Mars and Earth[39]. An impactor as large as the size of one Ceres (~1000 km diameter) is proposed to have struck early Mars to create its distinctive hemispheric crustal dichotomy in thickness and topography[40], and would have had profound shock pressure and thermal consequences for crustal minerals at all scales. We can place the time interval for the planet-shaping impactor collision at 4.51 ± 0.04 Ga based on the upper bracket of 4.55 Ga for first crust formation[28], and a lower bracket based on the weak shock and thermal metamorphic history of our samples of the secondary crust and its oldest concordant zircon age of 4.476 ± 0.001 Ga[28] (Fig. 2). This agrees with the minimum age bracket of 4.42 ± 0.07 Ga for dichotomy formation derived from Sm-Nd geochronology[41], with which, however, it was impossible to distinguish the cause for the dichotomy as due to mantle-overturn or giant impact[9]. Recent Lu-Hf chronological constraints show that mantle overturn was complete within 20 million years of planet formation[28] and thus falsify an endogenous origin for the dichotomy due to 1-degree (i.e., whole) mantle overturn, as the latter requires >100 million years to actuate[42]. It is possible that the zircon and baddeleyite crystallization events between 4.476 ± 0.001 Ga and 4.430 ± 0.001 Ga[28] represent the long period of crystallization following global melting of primary crust by the giant impact (Fig. 2) in view of the high impactor content of the igneous clasts[24].

This early, 4.51 ± 0.04 Ga age for the formation of the hemispheric dichotomy aligns with the period of Moon formation[4,5], and is a maximum age for habitability conditions (Fig. 2). In fact, it establishes the start of the very early time period for which volatiles, including water and organic compounds, could have been liberated and accumulated at the surface and in the near subsurface through volcanic processes[43,44] following giant impact. A global equivalent layer of water in the range of 229 meters is thought to have been present at the martian surface early in its history through such volcanic degassing[45], which is enough to account for some of the early water-related geomorphic features and may support the former presence of shallow seas. Our shock pressure reconstruction for this period indicates the existence of a weakly shocked crustal terrain that, in regard to pressure, was habitable from the beginning. The main threat from shock pressure to micro-organisms in the early crustal terrains would have been the mechanical shearing effects on cell walls[46], however such effects are well-known to be highly heterogeneous at the micro-scale[15]. Moreover, the terrain did not experience shock pressures >15 GPa, i.e. well below the known upper limit of viability of 78 GPa[7].

It appears therefore that temperature, rather than shock pressure, was the more important of the two factors limiting the onset of habitability of the early Mars crust. The two are tightly linked during the bombardment period and have been modelled with respect to crustal habitability volumes relative to early vs. late timing of peak impactor flux[3]. Our mineral evidence supports the 'classical post-accretion' model[3] of peak bombardment beginning at 4.57 Ga[47] with monotonic decline causing local impact-effects (e.g., our few shocked grains, Table S1), relict terrains unmodified by intense metamorphism, and crust viable for hyperthermophiles down to 8 km as early as 4.4 Ga. This is in line with U-Pu/Xe gas thermochronology results for whole rock samples of NWA 7034 that yield cooling as early as 4.319 ± 0.046 Ga below temperatures of at least ~450°C based on comparison with Pb behaviour in co-existing phosphates[9]. For the Rabt Sbayta polymict breccia we place a conservative age estimate of 4.2 Ga for the time at which the crustal fragments cooled to the thermal habitability window of ~160°C based on modeled rates of crustal thermal decay following post-accretion bombardment[3] (Fig. 2). We note that there is no evidence that our sample of the southern highlands of Mars suffered a later global, thermal or structural, modification of crust and hydrosphere by the putative 4.0 Ga to 3.8 Ga LHB[2]. For the Earth, the LHB is predicted to have been thermally cataclysmic for life, melting the outer crust down to 10 km, due to the cumulative effects of impact-triggered surface melting and pressure release melting from the early mantle[48] (Fig. 2). If indeed such an event occurred, its effects were not pervasive on Mars. This is consistent with dynamical modelling[49] and isotopic evidence[50] proposing either that Mars escaped an LHB, or, our favoured hypothesis, that genitive planet migration occurred within the first 100 million years of accretion[51] such that an LHB never took place.

The time window for abiogenesis on Mars could have been as long as 700 million years, from 4.2 to 3.5 Ga, based on evidence that the martian surface became much less hospitable by approximately 3.5 Ga[52,53]. This 700-million-year period is longer than Earth's Phanerozoic Eon, and more than the amount of time between accretion and the first signs of life on Earth at ~3.7 Ga[54]. Based on terrestrial geology, Mars' crust could pre-date the oldest known inhabited surface of Earth by half a billion years (Fig. 2). Alternatively, based on recent dynamical models[51], it is plausible that Earth, like Mars, experienced major bombardment only in the first ~100 million years, and likewise exhibited early habitable crustal platforms. Ar-Ar geochronology and cosmogenic nuclide exposure histories suggest that the earliest Mars crust fragments are derived from a terrain of hundreds of square kilometres which remained near the present surface[9] as opposed to having been deeply buried by later volcanism[28]. It is possible that this rock record of earliest habitability remains accessible in the modern martian crust and pertinent to future mission planning for sample return.

References:

1. Eigenbrode, J. L. *et al.* Organic matter preserved in 3-billion-year-old mudstones at Gale crater, Mars. *Science* **360,** 1096–1101 (2018).
2. Ryder, G. Mass flux in the ancient Earth-Moon system and benign implications for the origin of life on Earth. *J. Geophys. Res.* **107,** 5022 (2002).
3. Abramov, O. & Mojzsis, S. J. Thermal effects of impact bombardments on Noachian Mars. *Earth Planet. Sci. Lett.* **442,** 108–120 (2016).
4. Touboul, M., Kleine, T., Bourdon, B., Palme, H. & Wieler, R. Late formation and prolonged differentiation of the Moon inferred from W isotopes in lunar metals. *Nature* **450,** 1206–1209 (2007).
5. Barboni, M. *et al.* Early formation of the Moon 4.51 billion years ago. *Sci. Adv.* **3,** e1602365 (2017).
6. Gomes, R., Levison, H. F., Tsiganis, K. & Morbidelli, A. Origin of the cataclysmic Late

Heavy Bombardment period of the terrestrial planets. *Nature* **435,** 466–469 (2005).

7. Hazael, R., Meersman, F., Ono, F. & Mcmillan, P. F. Pressure as a limiting factor for life. *Life* **6,** 1–8 (2016).

8. Hazael, R., Fitzmaurice, B. C., Foglia, F., Appleby-Thomas, G. J. & McMillan, P. F. Bacterial survival following shock compression in the GigaPascal range. *Icarus* **293,** 1–7 (2017).

9. Cassata, W. S. *et al.* Chronology of martian breccia NWA 7034 and the formation of the martian crustal dichotomy. *Sci. Adv.* **4,** eaap8306 (2018).

10. Moser, D. E. *et al.* New zircon shock phenomena and their use for dating and reconstruction of large impact structures revealed by electron nanobeam (EBSD, CL, EDS) and isotopic U–Pb and (U–Th)/He analysis of the Vredefort dome. *Can. J. Earth Sci.* **48,** 117–139 (2011).

11. Kohn, M. J. & Kelly, N. M. in *Microstructural Geochronology: Planetary Records Down to Atom Scale* (eds. Moser, D. E., Corfu, F., Darling, J. R., Reddy, S. M. & Tait, K. T.) 35–61 (Wiley, 2017).

12. Heaman, L. M. & LeCheminant, A. N. Paragenesis and U-Pb systematics of baddeleyite (ZrO_2). *Chem. Geol.* **110,** 95–126 (1993).

13. Valley, J. W. *et al.* Hadean age for a post-magma-ocean zircon confirmed by atom-probe tomography. *Nat. Geosci.* **7,** 219–223 (2014).

14. Piazolo, S. *et al.* Deformation-induced trace element redistribution in zircon revealed using atom probe tomography. *Nat. Commun.* **7,** 10490 (2016).

15. Stöffler, D., Hamann, C. & Metzler, K. Shock metamorphism of planetary silicate rocks

and sediments: Proposal for an updated classification system. *Meteorit. Planet. Sci.* **53,** 5–49 (2018).

16. Crow, C. A., Moser, D. E. & McKeegan, K. D. Shock metamorphic history of >4 Ga Apollo 14 and 15 zircons. *Meteorit. Planet. Sci.* (2018).

17. El Goresy, A. Baddeleyite and its significance in impact glasses. *J. Geophys. Res.* **70,** 3453–3456 (1965).

18. Erickson, T. M. *et al.* Microstructural constraints on the mechanisms of the transformation to reidite in naturally shocked zircon. *Contrib. to Mineral. Petrol.* **172,** 6 (2017).

19. White, L. F. *et al.* Baddeleyite as a widespread and sensitive indicator of meteorite bombardment in planetary crusts. *Geology* **46,** 719–722 (2018).

20. Darling, J. R. *et al.* Variable microstructural response of baddeleyite to shock metamorphism in young basaltic shergottite NWA 5298 and improved U-Pb dating of Solar System events. *Earth Planet. Sci. Lett.* **444,** 1–12 (2016).

21. White, L. F. *et al.* Atomic-scale age resolution of planetary events. *Nat. Commun.* **8,** 15597 (2017).

22. Thomson, O. A. *et al.* Preservation of detrital shocked minerals derived from the 1.85 Ga Sudbury impact structure in modern alluvium and Holocene glacial deposits. *Bull. Geol. Soc. Am.* **126,** 720–737 (2014).

23. Agee, C. B. *et al.* Unique meteorite from early Amazonian Mars: Water-rich basaltic breccia Northwest Africa 7034. *Science* **339,** 780–785 (2013).

24. Humayun, M. *et al.* Origin and age of the earliest Martian crust from meteorite NWA 7533. *Nature* **503,** 513–516 (2013).

25. Wittmann, A. *et al.* Petrography and composition of Martian regolith breccia meteorite Northwest Africa 7475. *Meteorit. Planet. Sci.* **50,** 326–352 (2015).

26. Hewins, R. H. *et al.* Regolith breccia Northwest Africa 7533: Mineralogy and petrology with implications for early Mars. *Meteorit. Planet. Sci.* **52,** 89–124 (2017).

27. Bellucci, J. J. *et al.* A scanning ion imaging investigation into the micron-scale U-Pb systematics in a complex lunar zircon. *Chem. Geol.* **438,** 112–122 (2016).

28. Bouvier, L. C. *et al.* Evidence for extremely rapid magma ocean crystallization and crust formation on Mars. *Nature* **558,** 586–589 (2018).

29. McCubbin, F. M. *et al.* Geologic history of Martian regolith breccia Northwest Africa 7034: Evidence for hydrothermal activity and lithologic diversity in the Martian crust. *J. Geophys. Res. Planets* **121,** 2120–2149 (2016).

30. Cartwright, J. A., Ott, U., Herrmann, S. & Agee, C. B. Modern atmospheric signatures in 4.4 Ga Martian meteorite NWA 7034. *Earth Planet. Sci. Lett.* **400,** 77–87 (2014).

31. Lorand, J. P. *et al.* Nickeliferous pyrite tracks pervasive hydrothermal alteration in Martian regolith breccia: A study in NWA 7533. *Meteorit. Planet. Sci.* **50,** 2099–2120 (2015).

32. Roszjar, J., Moser, D. E., Hyde, B. C., Chanmuang, C. & Tait, K. in *Microstructural Geochronology: Planetary Records Down to Atom Scale* (eds. Moser, D. E., Corfu, F., Darling, J. R., Reddy, S. M. & Tait, K.) 113–135 (Wiley, 2017).

33. Moser, D. E. *et al.* Solving the Martian meteorite age conundrum using micro-baddeleyite and launch-generated zircon. *Nature* **499,** 454–457 (2013).

34. Wingate, M. T. D. & Compston, W. Crystal orientation effects during ion microprobe U–

Pb analysis of baddeleyite. *Chem. Geol.* **168,** 75–97 (2000).

35. Reinhard, D. A. *et al.* in *Microstructural Geochronology: Planetary Records Down to Atom Scale* (eds. Moser, D. E., Corfu, F., Darling, J. R., Reddy, S. M. & Tait, K.) 315–326 (Wiley, 2017).

36. Therriault, A. M., Grieve, R. A. F. & Reimold, W. U. Original size of the Vredefort Structure: Implications for the geological evolution of the Witwatersrand Basin. *Meteorit. Planet. Sci.* **32,** 71–77 (1997).

37. Crow, C. A., McKeegan, K. D. & Moser, D. E. Coordinated U–Pb geochronology, trace element, Ti-in-zircon thermometry and microstructural analysis of Apollo zircons. *Geochim. Cosmochim. Acta* **202,** 264–284 (2017).

38. Herd, C. D. K. *et al.* in *Microstructural Geochronology: Planetary Records Down to Atom Scale* (eds. Moser, D. E., Corfu, F., Darling, J. R., Reddy, S. M. & Tait, K.) 137–166 (Wiley, 2017).

39. Sleep, N. H. & Zahnle, K. Refugia from asteroid impacts on early Mars and the early Earth. *J. Geophys. Res.* **103,** 28529–28544 (1998).

40. Wilhelms, D. E. & Squyres, S. W. The martian hemispheric dichotomy may be due to a giant impact. *Nature* **309,** 138–140 (1984).

41. Nyquist, L. E. *et al.* Rb-Sr and Sm-Nd isotopic and REE studies of igneous components in the bulk matrix domain of Martian breccia Northwest Africa 7034. *Meteorit. Planet. Sci.* **51,** 483–498 (2016).

42. Watters, T. R., McGovern, P. J. & Irwin III, R. P. Hemispheres Apart: The Crustal Dichotomy on Mars. *Annu. Rev. Earth Planet. Sci.* **35,** 621–652 (2007).

43. Steele, A. *et al.* A Reduced Organic Carbon Component in Martian Basalts. *Science* **337,** 212–215 (2012).

44. Carr, M. H. & Head, J. W. Martian surface/near-surface water inventory: Sources, sinks, and changes with time. *Geophys. Res. Lett.* **42,** 726–732 (2015).

45. McCubbin, F. M. *et al.* Heterogeneous distribution of H_2O in the Martian interior: Implications for the abundance of H2O in depleted and enriched mantle sources. *Meteorit. Planet. Sci.* **51,** 2036–2060 (2016).

46. Horneck, G. *et al.* Microbial Rock Inhabitants Survive Hypervelocity Impacts on Mars-Like Host Planets: First Phase of Lithopanspermia Experimentally Tested. *Astrobiology* **8,** 17–44 (2008).

47. Bottke, W. F. & Andrews-Hanna, J. C. A post-accretionary lull in large impacts on early Mars. *Nat. Geosci.* **10,** 344–348 (2017).

48. Marchi, S. *et al.* Widespread mixing and burial of Earth's Hadean crust by asteroid impacts. *Nature* **511,** 578–582 (2014).

49. Brasser, R., Mojzsis, S. J., Werner, S. C., Matsumura, S. & Ida, S. Late veneer and late accretion to the terrestrial planets. *Earth Planet. Sci. Lett.* **455,** 85–93 (2016).

50. Dauphas, N. & Pourmand, A. Hf-W-Th evidence for rapid growth of Mars and its status as a planetary embryo. *Nature* **473,** 489–492 (2011).

51. Nesvorný, D., Vokrouhlický, D., Bottke, W. F. & Levison, H. F. Evidence for very early migration of the Solar System planets from the Patroclus – Menoetius binary Jupiter Trojan. *Nat. Astron.* **2,** 878–882 (2018).

52. Hurowitz, J. A. & McLennan, S. M. A ~ 3.5 Ga record of water-limited, acidic

weathering conditions on Mars. *Earth Planet. Sci. Lett.* **260,** 432–443 (2007).

53. Ehlmann, B. L. *et al.* The sustainability of habitability on terrestrial planets: Insights, questions, and needed measurements from Mars for understanding the evolution of Earth-like worlds. *J. Geophys. Res. Planets* **121,** 1927–1961 (2016).

54. Rosing, M. T. ^{13}C-Depleted Carbon Microparticles in >3700-Ma Sea-Floor Sedimentary Rocks from West Greenland. *Science* **283,** 674–676 (1999).

Corresponding Author: All correspondence and requests for materials should be addressed to Prof. Desmond Moser, Dept. of Earth Sciences, University of Western Ontario, London, Ontario, Canada N6A 5B7 ; email: desmond.moser@uwo.ca

Acknowledgments:

Non-Author contributions: The following curators/institutions are gratefully acknowledged for providing sample material; B. Hofmann (Naturhistorisches Museum Bern, CH) for loan of NWA 7906, John Kashuba for loan of the NWA 11220 thin sections, and Ben Hoefnagels for loan of Rabt Sbayta 003. The following are gratefully acknowledged for their assistance with making or running atom probe tomography specimens; Ty Prosa, Isabelle Martin, Katherine P. Rice, Yimeng Chen, Dave Olson, and Daniel Lawrence.

Funding:

DEM acknowledges support for electron microscopy analyses, student and technical scientist funding, and facility travel costs from his NSERC Discovery Grant; JRD acknowledges support from Royal Society Research Grant RG160237 and a University of Portsmouth RIEF award;

FMM acknowledges support from NASA's Planetary Science Research Program; KTT acknowledges NSERC Discovery Grant support.

Author contributions: DEM was in charge of conceptualization of the project and writing the initial draft. All authors provided support in one or more of these roles; investigation, formal analysis, resource provision, and written contributions to subsequent drafts of the manuscript. AJI was the classifier of two of the specimens used in this study and provided thin and thick sections for detailed analyses.

Competing interests: Authors declare no competing interests. We note that the CAMECA co-authors (DR and DL) are engaged in the manufacture and sale of atom probe instruments.

Materials and Methods

Electron microscopy

Petrographic slabs, thick and thin sections were created from the collected samples using standard sample preparation techniques[29]. Sections were subjected to a final polishing step using a colloidal silica solution (0.05 µm, pH 8.5) and a vibratory polisher. Electron microscopy was performed with a Hitachi SU6600 field emission scanning electron microscope (FE-SEM; Schottky emitter) located in the Zircon and Accessory Phase Laboratory at the University of Western Ontario, London, Ontario. Features of interest (e.g., zircon and baddeleyite) were initially located using backscatter electron (BSE) imaging (five segment solid-state detector) and energy dispersive spectroscopy (EDS; Oxford X-max 80 mm2 silicon drift detector) within Oxford INCA's Feature mapping routine, at an accelerating voltage of 15 kV; these features were subsequently overlain on BSE/EDS section montages by plotting the feature's stage coordinates using Esri's ArcGIS.

Automated SEM-BSE-EDS mapping was used to identify target grain locations and dimensions prior to characterizing micro- and nano-scale features. Many hundreds of grains, mostly in the 1 µm to 9 µm size range, were detected and are mostly angular fragments in the breccia matrix. The size fraction larger than 10 µm in maximum dimension (n = 147) (Table S1) was examined using electron microscopy, including Secondary Electrons (SE), Backscattered Electrons (BSE), Cathodoluminescence (CL), and Electron Backscatter Diffraction (EBSD), to determine internal zoning patterns, lattice orientation microstructure, crystallinity, and any metamorphic polymorphs (e.g., reidite) or phase-transition heritage. There is no directional fabric in the grain populations, and hence the analyzed surfaces include random intersections of larger (>50 µm) grains such as those liberated by crushing[28] and shown on some surfaces (e.g., Fig. S4).

Each crystalline grain (n = 121 for martian samples) was examined using BSE and/or CL for microscopic primary features, secondary metamorphic features[11], and the suite of shock metamorphic indicators described above. The largest (by length) features of each sample were extensively imaged using secondary electron (SE), BSE, and EDS point analysis to capture morphology and associated phases. Several of those grains were then analyzed further using other methods, including EDS mapping, cathodoluminescence (CL) and electron backscatter diffraction (EBSD). Colour CL images were collected for all but NWA 7906 with a customized Gatan ChromaCL RGB+UV detector system and Gatan Digital Micrograph software, using a 10 kV electron beam and 250 us pixel time. Microstructural EBSD orientation data was captured with an Oxford Nordlys detector and HKL's Channel5 software. Samples were tilted to 70^o within the SEM chamber and raised to a working distance of 19.0 mm. Kikuchi patterns were generated using a 20 kV, 8.0 nA electron beam, and captured using the camera settings of 24 ms/frame acquisition time, 4x4 pixel binning, high gain, and frame averaging of 7. Patterns were then indexed using a minimum of five and a maximum of seven Kikuchi bands, and a Hough transform resolution setting of 60. Beam step-sizes during mapping were 60nm to 125 nm but most commonly = 125nm. A mean angular deviation (MAD) discriminator was set to a value of 1.5, above which analyses were assigned a zero solution to avoid indexing of poor quality EBSPs. Post-analysis noise reduction processing was not applied to any of the data sets other than removing erroneous "wild spikes". Orientation microstructure and crystallographic analysis by EBSD was used to evaluate pre- and post-launch shock-induced microstructures and search for signs of high-pressure polymorphs or their reversion products. The same instruments and procedures were used for the shock microstructural survey of zircons in petrographic thin sections across the Vredefort impact structure (Table 1) as detailed in the source M.Sc. thesis by C. Davis (https://ir.lib.uwo.ca/etd/4185/). NWA 7906 was analyzed at the Natural History Museum Vienna, Austria. CL images were obtained using a Gatan MonoCL (MonoCL4R) system attached to a JEOL JSM 6610-LV SEM. Monochromatic images are obtained by using wavelength-filtered (monochromatic) red (R)-green (G)-–blue (B) setting that yield false-color (composite) RGB images, while panchromatic (gray-scale) images result from the integration of the luminescence over all emissions. Operating conditions for all SEM-Mono CL images were 15 kV accelerating voltage, 1.2 nA beam current, and a working distance of ~11 mm.

<u>Atom probe tomography (APT)</u>

APT allows the three-dimensional mapping and identification of elements and isotopes within minerals[13], APT data sets were prepared by gallium focused ion beam milling at CAMECA® Instruments Inc., Madison, Wisconsin. Standard liftout and mount techniques were used to produce the desired specimen shape with a radius of curvature < 100 nm[55,56]. A final low voltage (10 kV) milling step was preformed to help minimize gallium implantation and damage. Prepared microtips were analyzed at CAMECA using a LEAP® 4000X HR™ atom probe equipped with a reflectron flight path and operating in laser pulsed mode. Field evaporation of each microtip was induced under ultrahigh vacuum by applying a high electric field (achieved by applying 4-12 kV) at cryogenic conditions (~50–60 K) to the specimen apex. In laser pulse mode, ionization and evaporation of atoms on the specimen surface was promoted by an ultraviolet laser (355 nm wavelength) with pulse energies and frequencies that varied between ~100–400 pJ and ~150–200 kHz, respectively. During acquisition, the mass-to-charge ratio of the ions is determined through time–of–flight mass spectrometry by measuring the time from field evaporation to detection and equating it to their kinetic energy. A spatial reconstruction of the specimen is achieved by projecting the ions from a position–sensitive detector back to the tip apex and considering the sequential order of evaporation. Complete detail on data acquisition and reconstruction with the local electrode atom probe are described elsewhere[57].

Data analysis and ranging of mass spectra were conducted using the Cameca IVAS™ 3.6.12 software. For each microtip dataset, corrected ionic counts of major and trace elements were calculated through the subtraction of background counts from the raw ionic counts. Background counts were measured using the local range–assisted background model in IVAS. In all scenarios, the peak locations of trace element (e.g., Y, Fe, Al, U and Pb) were identified within each microtip spectrum using the BR266 zircon standard and baddeleyite standard Phalaborwa as reference[35]. For individual peaks, range bounds were set by eye from baseline to baseline to encompass the entirety of each peak[21]. It is noted here however, that there are no standard protocols with which to set range widths, and it is a key source of variation that is actively being explored in the field (eg.,[57,58]). Details on acquisition and spatial reconstruction parameters selected for this work are given in Supplementary Data Table 3.

Data and materials availability: All data is summarized and available in the main text or the supplementary materials. Raw instrument data is available to editors and reviewers upon request.

References:

55. Larson, D. J. *et al.* Field-ion specimen preparation using focused ion-beam milling. *Ultramicroscopy* **79,** 287–293 (1999).

56. Thompson, K. *et al.* In situ site-specific specimen preparation for atom probe tomography. *Ultramicroscopy* **107,** 131–139 (2007).

57. Larson, D. J., Prosa, T. J., Ulfig, R. M., Geiser, B. P. & Kelly, T. F. *Local Electrode Atom Probe Tomography*. (Springer, 2013).

58. Blum, T. B. *et al.* in *Microstructural Geochronology: Planetary Records Down to Atom Scale* (eds. Moser, D. E., Corfu, F., Darling, J. R., Reddy, S. M. & Tait, K.) 237–350 (Wiley, 2017).

Figure Captions:

Fig. 1. Example of early Mars crust and igneous zircon in polymict breccia meteorite NWA 11220; (a) optical micrograph showing twinned plagioclase (grey and white banding), orthopyroxene (yellow) and clinopyroxene (red/blue). (b) Higher magnification EBSD lattice orientation map (white box in (a)) indicating highly crystalline minerals coloured according to Euler angle relative to sample urface, except for zircon grain (red), coloured according to crystal axis parallel to surface. (c) highest magnification SE and CL images, and EBSD orientation map, for euhedral, igneous zircon illustrating launch-related [<15 GPa[25]] open fractures (white arrow).

Such grains testify to the absence of major shock metamorphic effects on the source crust domain since ≥4.43 billion years ago.

Fig. 2. Timeline of early Mars bombardment history and habitability compared to Earth. Timing of major events in the early histories of Mars and Earth showing the classical post-accretion bombardment flux curve[3] (red dashes), and an early period of planet-scale impact effects such as formed the hemispheric dichotomy; both dictated by the existence of ≤4.476 ±0.001 Ga grains of zircon and baddeleyite grains and host crust, unaltered by shock metamorphism >20 GPa on Mars. Note that the Mars giant impact period overlaps current age estimates for Moon formation. Early Mars crust was below shock pressure habitability after this time. Thermal habitability of early Mars crust was possible at 4.4 Ga[3], and based on the oldest U-Pu/Xe cooling date of 4.32 Ga for our samples[9] we estimate that the source crustal terrane was habitable by 4.2 Ga, a time of accelerated volatile release following dichotomy formation. Our samples of Mars crust did not experience later, pervasive cataclysm at ~3.9Ga during the putative late heavy bombardment (LHB)[6]. Habitable crust on Mars predates Earth's oldest known biosignatures[54] by as much as ~500 million years. The absence of shock metamorphic features in Hadean Earth zircon[13] and recent dynamical modelling[51] allow that Earth also had opportunity for early abiogenesis. Inset: NASA-MOLA false-color topographic model of the Mars surface showing the hemispheric dichotomy and southern highlands (orange), a likely source for the Martian polymict breccia meteorites[24–26].

Table 1. Results of in-situ shock microstructural analyses of zirconium minerals in polished sections of bombarded crust from across the central uplift of the Vredefort impact structure compared to early Mars samples. Earth values similar to Moon results (see text) (*) Shock metamorphism is characterized by the occurrence of any of the following features; planar or curviplanar features, impact-melt glass inclusions, crystal plastic deformation, high pressure polymorphs or reversion products thereof, granularization or neobastic growth, and nano-scale clustering of trace elements.

Vredefort (Earth) Samples	Distance from center of impact	Coordinates (UTM)		Total grains	# shock metamor-phosed*	% shock metamor-phosed*
V15-39	~5 km	543699 m E	7014140 m S	45	42	94
V15-16	~8.6 km	540091 m E	7010527 m S	48	48	100
V49-1	~8.9 km	542531 m E	7015741 m S	41	37	90
V15-46	~17.1 km	539943 m E	7025719 m S	48	41	85
V-62	~22.8 km	534627 m E	7029025 m S	33	32	97
V15-55	~24.5 km	563809 m E	7030330 m S	36	18	50
Total	-	-	-	**251**	**218**	**87%**
Mars samples; NWA 7034, 7475, 7906, 11220, Rabt Sbayta 003						
Total		-	-	**121**	**3**	**2%**

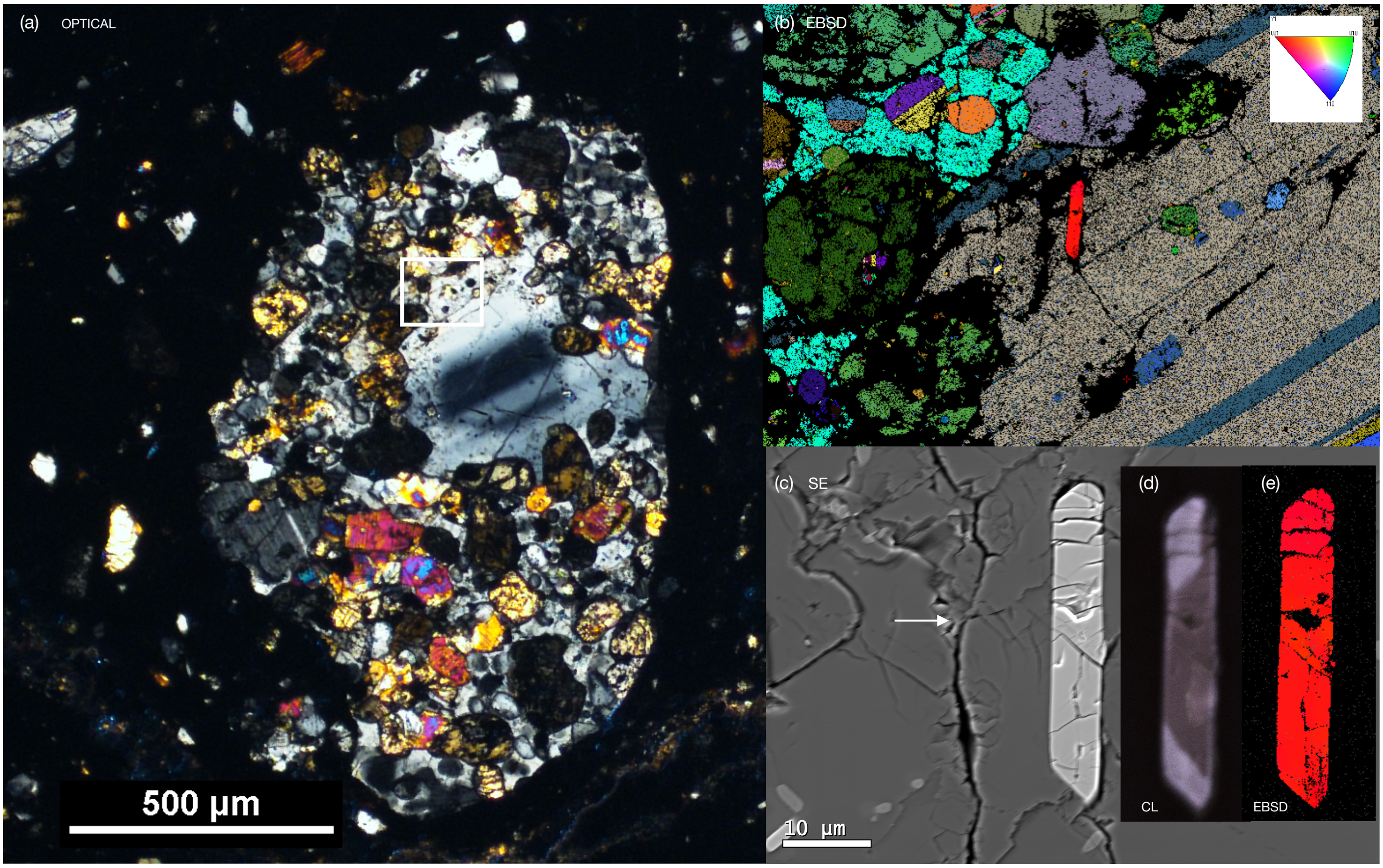

Figure 1. Moser et al. ; NGS-2018-09-02050A Mar 27, 2019

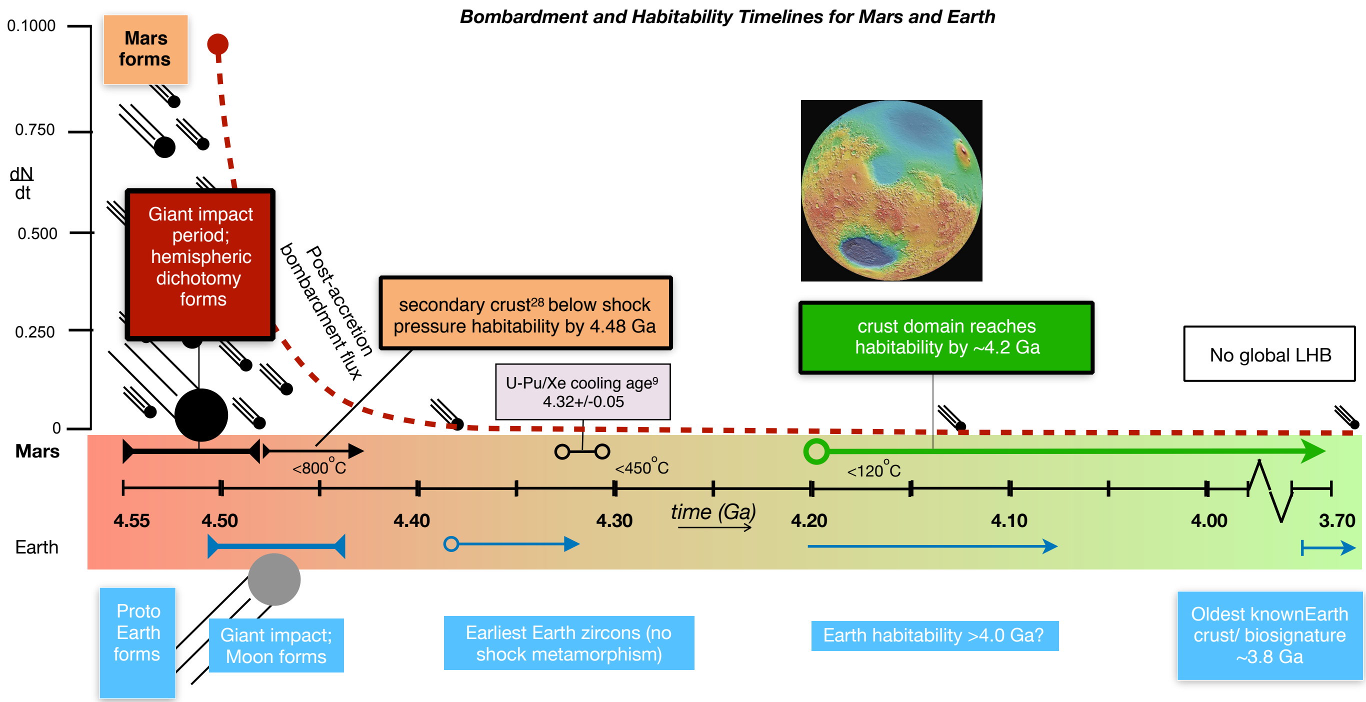

Figure 2. Moser et al. ; NGS-2018-09-02050A Mar 27, 2019